JARO
Journal of the Association for Research in Otolaryngology

High-Frequency Force Generation in the Constrained Cochlear Outer Hair Cell: A Model Study

Zhijie Liao,[1] Aleksander S. Popel,[1] William E. Brownell,[2] and Alexander A. Spector[1]

[1]*Department of Biomedical Engineering, Johns Hopkins University School of Medicine, Baltimore, MD 21205, USA*
[2]*Bobby R. Alford Department of Otorhinolaryngology and Communicative Sciences, Baylor College of Medicine, Houston, TX 77030, USA*

ABSTRACT

Cochlear outer hair cell (OHC) electromotility is believed to be responsible for the sensitivity and frequency selectivity of the mammalian hearing process. Its contribution to hearing is better understood by examining the force generated by the OHC as a feedback to vibration of the basilar membrane (BM). In this study, we examine the effects of the constraints imposed on the OHC and of the surrounding fluids on the cell's high-frequency active force generated under *in vitro* and *in vivo* conditions. The OHC is modeled as a viscoelastic and piezoelectric cylindrical shell coupled with viscous intracellular and extracellular fluids, and the constraint is represented by a spring with adjustable stiffness. The solution is obtained in the form of a Fourier series. The model results are consistent with previously reported experiments under both low- and high-frequency conditions. We find that constrained OHCs achieve a much higher corner frequency than free OHCs, depending on the stiffness of the constraint. We analyze cases in which the stiffness of the constraint is similar to that of the BM, reticular lamina, and tectorial membrane, and find that the force per unit transmembrane potential generated by the OHC can be constant up to several tens of kHz. This model, describing the OHC as a local amplifier, can be incorporated into a global cochlear model that considers cochlear hydrodynamics and frequency modulation of the receptor potential, as well as the graded BM stiffness and OHC length.

Keywords: mathematical model, electromotility, active force, piezoelectric

INTRODUCTION

The mammalian cochlear outer hair cell (OHC) plays a key role in amplification and frequency discrimination during hearing. This phenomenon, called the cochlear amplifier, is most pronounced under high-frequency conditions when the active properties of the OHC must overcome the viscous drag forces caused by the relative movement of the fluid and solid components of the cochlea. There is a natural frequency modulation (filtering) of sound transduction in the cochlea, and the mechanical component of this frequency modulation is associated with the effect of the viscous drag forces.

The viscous resistance to the movement of the cochlear components was the primary concern in the first proposal of the active cochlea (Gold 1948). Inside the cochlea, the OHCs are located between the overlying reticular lamina (RL) and tectorial membrane (TM) complex, and the underlying Deiters' cell (DC) and basilar membrane (BM) complex. The constraints imposed on the OHC by these components of the cochlea determine the amount of the OHC movement that causes the drag (shear) forces on the surface of the cell.

It is believed that OHC electromotility (Brownell et al. 1985) is critically important for the active properties of the OHC. In this mechanism, an uncon-

Correspondence to: Zhijie Liao · Department of Biomedical Engineering · Johns Hopkins University · 720 Rutland Ave., 613 Traylor Bldg., Baltimore, MD 21205, USA. Telephone: +1-410-9551787; fax: +1-410-6148796; email: zliao@jhu.edu

strained OHC changes its length, and a constrained OHC generates a force in response to changes in the cell's transmembrane potential. The force produced by the OHC is fed back to the vibrating BM, and, as a consequence, the movement of the BM is adjusted to enhance the sensitivity and frequency selectivity. Thus, the OHC's high-frequency force is a key element of active hearing.

The OHC undergoes dimensional changes in response to electrical stimulation (Brownell et al. 1985) and, conversely, electric current is generated across the membrane in response to cell deformation (Gale and Ashmore 1994). This coupled electromechanical behavior suggests that the OHC can be treated as a piezoelectric-type actuator (Steele et al. 1993; Mountain and Hubbard 1994). Recent studies have identified a protein prestin, which is located in the OHC basolateral membrane; together with chloride ions, prestin plays a central role in the phenomenon of OHC electromotility and active force production (Zheng et al. 2000; Oliver et al. 2001; Liberman et al. 2002).

The force generated by OHCs has already been studied in both experiments and models. Hallworth (1995, 1997) used a suction pipette to hold the basal end of the OHC and measured the force generated by applying a glass fiber against the OHC's apical end. Iwasa and Adachi (1997) chose the whole-cell voltage clamp technique to examine force generation. All of these force measurements were performed under low-frequency conditions. Frank et al. (1999) applied the microchamber setup (Dallos et al. 1993; Dallos and Evans 1995) and, for the first time, measured the OHC high-frequency active force generation. They have demonstrated (see also Scherer and Gummer 2004) that the force generated by the OHC can be constant up to tens of kHz.

Several models have also been developed (Hallworth 1995; Iwasa and Adachi 1997; Spector et al. 1999) to predict the OHC active force generation under low- and moderate-frequency conditions.

Tolomeo (1995) and Tolomeo and Steele (1998) applied the Fourier series technique to investigate length change in a free OHC in response to high-frequency mechanical and electrical stimuli. They found that viscous damping cannot be ignored in the high-frequency performance of the cell, and the movement of the cell wall is coupled with that of the viscous intracellular and extracellular fluids. Ratnanather et al. (1997) considered both the viscosity of the fluids and that of the cell wall.

In addition to characterizing the high-frequency force production in response to prescribed changes in the transmembrane potential (force per unit transmembrane potential), it is also important to understand how these changes in the potential

(receptor potentials) are delivered under physiological conditions. Although high-frequency receptor potentials have not been measured, a simple model using electrical properties (resistance and capacitance) of the OHC membrane predicted a severe attenuation of the receptor potential (Santos-Sacchi 1992; Housley and Ashmore 1992). Subsequent estimates showed that receptor potentials can be significantly higher than those predicted on the basis of conventional electrical properties of the cell membrane. Dallos and Evans (1995) suggested that the OHC *in vivo* is driven by an extracellular electric field. This concept was recently analyzed by Fridberger et al. (2004), who simultaneously measured the velocity of the basilar membrane and the electric potential inside the organ of Corti in response to acoustic stimulation. Recently, several studies (Santos-Sacchi et al. 1998; Spector et al. 2002, 2003; Ospeck et al. 2003; Weitzel et al. 2003; Rybalchenko and Santos-Sacchi 2003; Rabbitt et al. 2005) performed finer analyses of the biophysical properties of the OHC membrane that resulted in greater receptor potentials than those predictions based on RC analysis.

In the present study, we concentrate on the mechanical effects, the viscous drag (shear) forces, and constraints imposed on the OHC, on active force production under high-frequency conditions. Thus we focus on the mechanical component of the frequency modulation in the cochlea. We do not consider here the frequency modulation of the receptor potential, and our current results are expressed in terms of the active force per unit transmembrane potential. The total active force can be found as the product of the force per unit transmembrane potential estimated here and the receptor potential if the latter potential is derived from an independent analysis. The proposed model can cover both experimental and physiological conditions.

We modeled the constrained OHC as a circular cylinder held by a micropipette (microchamber) and attached to a spring at the other end. The viscous intracellular and extracellular fluids and the viscoelastic and piezoelectric cell's lateral wall are coupled. By choosing to make the stiffness of the spring equal to that of the glass fiber or to that of the cochlear components, we were able to model experimental conditions or make predictions regarding the OHC active force production *in vivo*, respectively. The force predicted by our model was consistent with the experimental results of Hallworth (1995), Iwasa and Adachi (1997) and Frank et al. (1999). We found that the constrained OHC could achieve a much higher corner frequency than the free OHC, and that the force per unit transmembrane potential *in vivo* could be constant up to a few tens of kHz. The

proposed model can lead to a better understanding of the mechanics underlying OHC high-frequency electromotility.

MODEL

Major equations

In our analysis, the cell wall is under the action of the applied electric field. In addition to that, the extracellular and intracellular fluids interact with the cell wall via surface forces (tractions). These external forces are balanced by the forces (resultants) inside the cell wall. The resultants are related to the strain and strain rate through viscoelastic constitutive equations. We assume steady-state harmonic and axisymmetric vibration of the cell and present the amplitude of all cellular characteristics in terms of Fourier expansion with respect to the x-coordinate (Fig. 1). We transform the original equations and express the cell's end displacement

in terms of the "generalized stiffness matrix" of the system that includes the cell wall and two fluids. The coefficients of that matrix are determined by the viscoelastic moduli of the cell wall, as well as by the viscous and inertial properties of the fluids. Finally, we compute the active force as the product of the cell end displacement and the stiffness of the constraint.

The constitutive equations for the cell wall that include the orthotropic elastic, viscous and piezo-electric components (Tolomeo 1995; Ratnanather et al. 1997; Tolomeo and Steele 1998) take the form

$$
\begin{bmatrix} N_x \\ N_\theta \end{bmatrix} = \begin{bmatrix} C_{11} & C_{12} \\ C_{12} & C_{22} \end{bmatrix} \begin{bmatrix} \frac{\partial u_x}{\partial x} \\ \frac{u_r}{r_c} \end{bmatrix}
$$
$$
+ \begin{bmatrix} \eta & -\eta \\ -\eta & \eta \end{bmatrix} \begin{bmatrix} \frac{\partial^2 u_x}{\partial x \partial t} \\ \frac{\partial u_r}{r_c \partial t} \end{bmatrix} + V \begin{bmatrix} e_x \\ e_\theta \end{bmatrix}, \quad (1)
$$

where N_x and N_θ are the components of the stress resultant (i.e., the product of the stress and cell wall
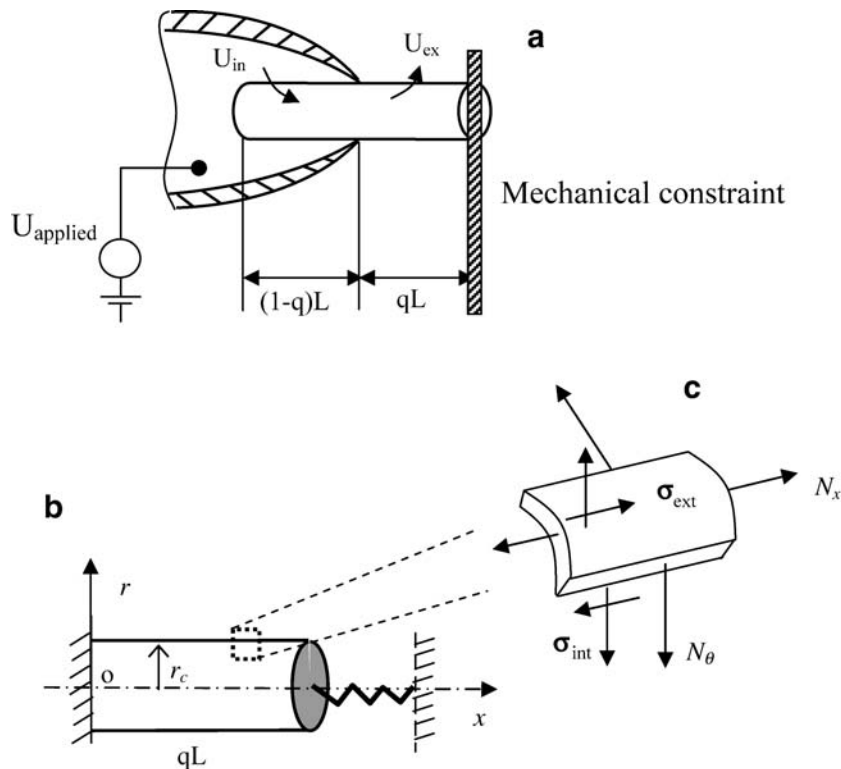

FIG. 1. Modeling constrained OHC. (a) Force measurement in the microchamber experiment. Mechanical constraint was either a lever or a glass probe with one end fixed and the other end attached to the OHC. q is the exclusion ratio (excluded cell length/total cell length), L is the whole length of the cell, $U_{applied}$ is the applied voltage; the transmembrane voltage change in the excluded and included cell parts are $U_{ex} = (1 - q)U_{applied}$ and $U_{in} = -qU_{applied}$, respectively. (b) The cell is modeled as a cylindrical shell coupled with intracellular and extracellular fluids. One cell end is fixed, and the

other cell end is connected to a spring simulating the mechanical loading. r_c is the radius of the cell. (c) σ_{int} and σ_{ext} represent the tractions on the cell wall surface due to the intracellular and extracellular fluids, respectively. σ_{int} and σ_{ext} are in the vector form, each with two components in the longitudinal and radial directions. The resultant (N_x, N_θ) generated in the cross-section of cell wall is a consequence of the extracellular and intracellular fluid tractions $(\sigma_{ext} - \sigma_{int})$, mechanical constraint (the spring), closed end, and electrical stimulation of the cell.

thickness) normal to the corresponding cross sections of the cell wall (Fig. 1); the subscripts r, x, and θ indicate the radial, axial, and circumferential directions, respectively; C's are the stiffness moduli; u_x and u_θ are two components of the wall displacement; η is the cell wall viscosity; t is time; r_c is the cell radius; V is the transmembrane potential change; and e_x and e_θ are two coefficients that determine the production of the local active force (resultant) per unit transmembrane potential (Spector et al. 1998, 1999; Spector and Jean 2003).

The movement of the intracellular and extracellular fluids is governed by linearized Navier–Stokes equations (Tolomeo 1995; Tolomeo and Steele 1998):

$$-\nabla p + \mu \nabla^2 \mathbf{v} = \rho \frac{\partial \mathbf{v}}{\partial t}, \qquad (2)$$

where p is the pressure, μ is the fluid viscosity, $\mathbf{v}$ is the velocity in the vector form (here and later, the vectors and matrices are written in boldface), and ρ is the fluid density. To characterize the interaction between the fluids and cell wall, we use no-slip boundary conditions in which the velocities of fluids and cell wall at interacting surfaces are equal.

The cap at the end of the cylindrical cell is treated as an oscillating rigid plate immersed in the fluid that will add extra hydrodynamic resistance to the cell wall (Zhang and Stone 1998). Also, additional terms associated with the effect of the constraint (spring) are considered.

The tractions and displacements can be expressed as the Fourier series in the cell wall and fluid domains. The Fourier series is then substituted into the governing Eqs. (1) and (2) for the cell wall and fluid, respectively. As a result of these derivations, the solution in terms of the Fourier coefficients of the cell wall displacement is obtained as follows:

$$\mathbf{F}_u = -\mathbf{B}^{-1}\mathbf{F}_\sigma^{piez}, \qquad (3)$$

where $\mathbf{F}_u$ and $\mathbf{F}_\sigma^{piez}$ are, respectively, the vectors of the Fourier coefficients of the cell wall displacement and the resultant caused by the electrical stimulation of the cell. $\mathbf{B}$ is the generalized stiffness matrix given by the equation:

$$\mathbf{B} = \mathbf{k}_{cell} + \mathbf{k}_{fluid} + \mathbf{k}_{end} + \mathbf{k}_{spring}, \qquad (4)$$

where $\mathbf{k}_{cell}$, $\mathbf{k}_{fluid}$, $\mathbf{k}_{end}$, and $\mathbf{k}_{spring}$ are the matrices associated with the cell wall, fluids, closed end, and constraint, respectively. Note that the generalized stiffness matrix reflects not only the elastic properties of the cell wall and the constraint but also the viscous

and inertial properties of the fluids. More details about these derivations are given in the Appendix.

We can then compute the amplitude of cell end displacement u_{end} by using the previously found vector $\mathbf{F}_u$ of the Fourier coefficients. The amplitude ($|u_{end}|$) of cell end displacement is the amplitude of the sum of Fourier series given by Eq. (A6) in the Appendix and estimated at the location of the cell end.

Finally, the amplitude of the force acting on the constraint is obtained as

$$F_{end} = k_{constr}|u_{end}|, \qquad (5)$$

where k_{constr} is the stiffness of the cell constraint, represented by a spring attached at the cell's end. The force given by Eq. (5) is equal to the active force generated by the cell as a result of its electrical stimulation.

Model parameters

The elastic moduli and coefficients of the electromotile response for the cell wall are chosen as C_{11} = 0.096 N/m, C_{12} = 0.16 N/m, C_{22} = 0.3 N/m, e_x = 0.0029 N/Vm and e_θ = 0.0018 N/Vm (Spector et al. 1998, 1999; Spector and Jean 2003).

The precise wall viscosity of the OHC is not currently available. We assume that this viscosity is on the order of 1×10^{-7} Ns/m, similar to that of the red blood cell membrane (Evans and Skalak 1980). This assumption is based on an important contribution of spectrin networks to the viscosities of both cells. The spectrin cytoskeleton is the predominant determinant of the viscosity of the red blood cell (Evans and Skalak 1980). The cytoskeleton of the OHC is also probably the most viscous component of the cell (the remaining components of the cell's composite wall are membranous structures and the fluid in the extracisternal space). The spectrin cross-links in the OHC cytoskeleton are oriented parallel to the axial direction, in which cell vibration is constrained. Therefore, they are likely to make the most significant contribution to the viscous damping of the cell wall's movement.

The intracellular fluid viscosity of the OHC has not yet been measured experimentally. Fung (1993) mentioned that the intracellular fluid viscosity in some cells is 5 to 6 times greater than the water viscosity. Luby-Phelps (2000) reported a cytoplasmic viscosity within a range of $(1.0–10.0) \times 10^{-3}$ Ns/m^2. Here, we have chosen to assign an internal fluid viscosity of 6.0×10^{-3} Ns/m^2 to the OHC. Using this value as a reference, we evaluated a range of values ($(1.0–10.0) \times 10^{-3}$ Ns/m^2) to assess the sensitivity to this parameter.

Effective cell length (μm)	Probe stiffness (N/m)	End displacement (nm/mV)	Probe force (pN/mV)	Isometric force (pN/mV)
41	0.0025	5.70 (6.16 ± 2.65)	14 (15 ± 7)	61 (91 ± 25)
47	0.0028	6.13 (7.95 ± 1.95)	17 (22 ± 5)	61 (116 ± 31)
46	0.0046	5.12 (6.75 ± 2.03)	24 (31 ± 9)	61 (104 ± 47)

In the last three columns of this table, Iwasa and Adachi's (1997) results (their Table 1) are included in parentheses, whereas the model results are outside the parentheses. Effective cell length is the distance between the patch pipette (located above nucleus) and the cell's apical end. Our model results are in good agreement with experimental results.

RESULTS AND DISCUSSION

Comparison with previous experimental data

Table 1 and Figure 2 compare our model results with data from the available low-frequency experiments. Iwasa and Adachi (1997) used the whole-cell voltage clamp technique to deliver voltage pulses through a patch pipette to induce OHC electromotility. Force was generated when a glass fiber was attached to the cell end. We found that the cell's end displacement and force predicted by our model agreed well with these previously published experimental results (Table 1). Our model predicted 14, 17, and 24 pN/mV (column 4 in Table 1), as compared to the corresponding ranges measured in the experiment, 15 ± 7, 22 ± 5 and 31 ± 9 pN/mV (Iwasa and Adachi 1997). Thus, it appears that our model prediction is close to the lower end of these experimental results. Increasing the fiber stiffness produced an increase in the

force but a decrease in the displacement. Our model can also be used to predict isometric force by assigning a very large value for fiber stiffness (e.g., 1000 N/m). The result we obtained was 61 pN/mV, which is also at the lower end of the range of active force estimated by Iwasa and Adachi (1997), whose mean value was approximately 100 pN/mV. Our model results also indicated that the isometric active force was independent of the cell length.

Hallworth (1995) used a suction pipette to hold the basal end of the OHC and deliver the command voltage. A fiber provided mechanical loading with varying levels of stiffness when the apical end of the OHC was placed against different parts of the fiber. The experimental results in Hallworth's study ranged from 0.01 to 100 pN/mV, but most were below 20 pN/mV. Figure 2 compares our model results with those of Hallworth (1995) when the loading stiffness was 1.60 mN/m. Our model results fell into the range measured by Hallworth and also showed that the force [which corresponds to a finite stiffness of the constraint (fiber)] increased with cell length. The inset table in Figure 2 also compared our model prediction with the value calculated from the regression equation (force = −8.263 + 0.438 × cell length, and R^2 = 0.284) for experimental data (Hallworth 1995). When the cell length is 40 μm, our model result is 9.4 pN/mV, in agreement with the 9.3 pN/mV calculated from the regression equation. If the cell length is shorter than 40 μm, our model prediction is larger than that from experimental regression equation (7.4 vs. 4.9 pN/mV for a 30-μm cell). However, if the cell length is longer than 40 μm, our model result is smaller than that from experimental regression equation (11.2 vs. 13.6 pN/mV for a 50-μm cell, and 12.9 vs. 18.0 pN/mV for a 60-μm cell). Given the relatively scattered experimental data, our model results are consistent with Hallworth's (1995) data.
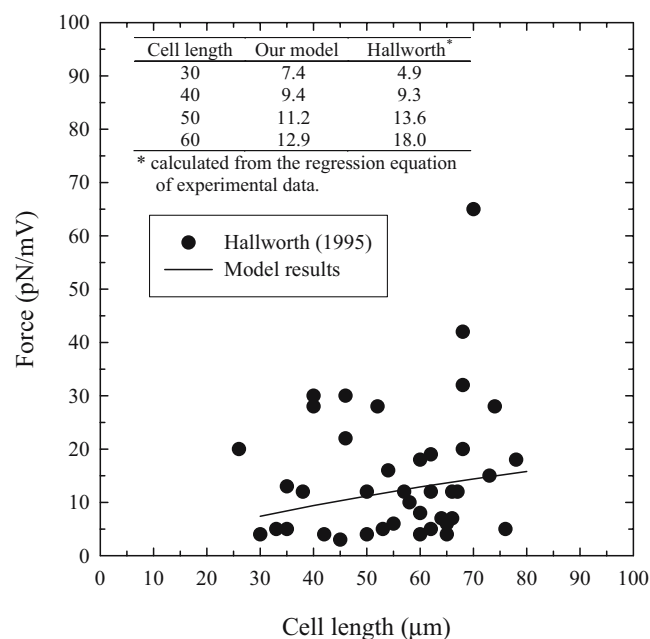

FIG. 2. Model results compared to Hallworth's (1995) experiment. The cell radius was 4 μm, and the loading fiber stiffness was 1.60 mN/m.

Effect of the constraint stiffness

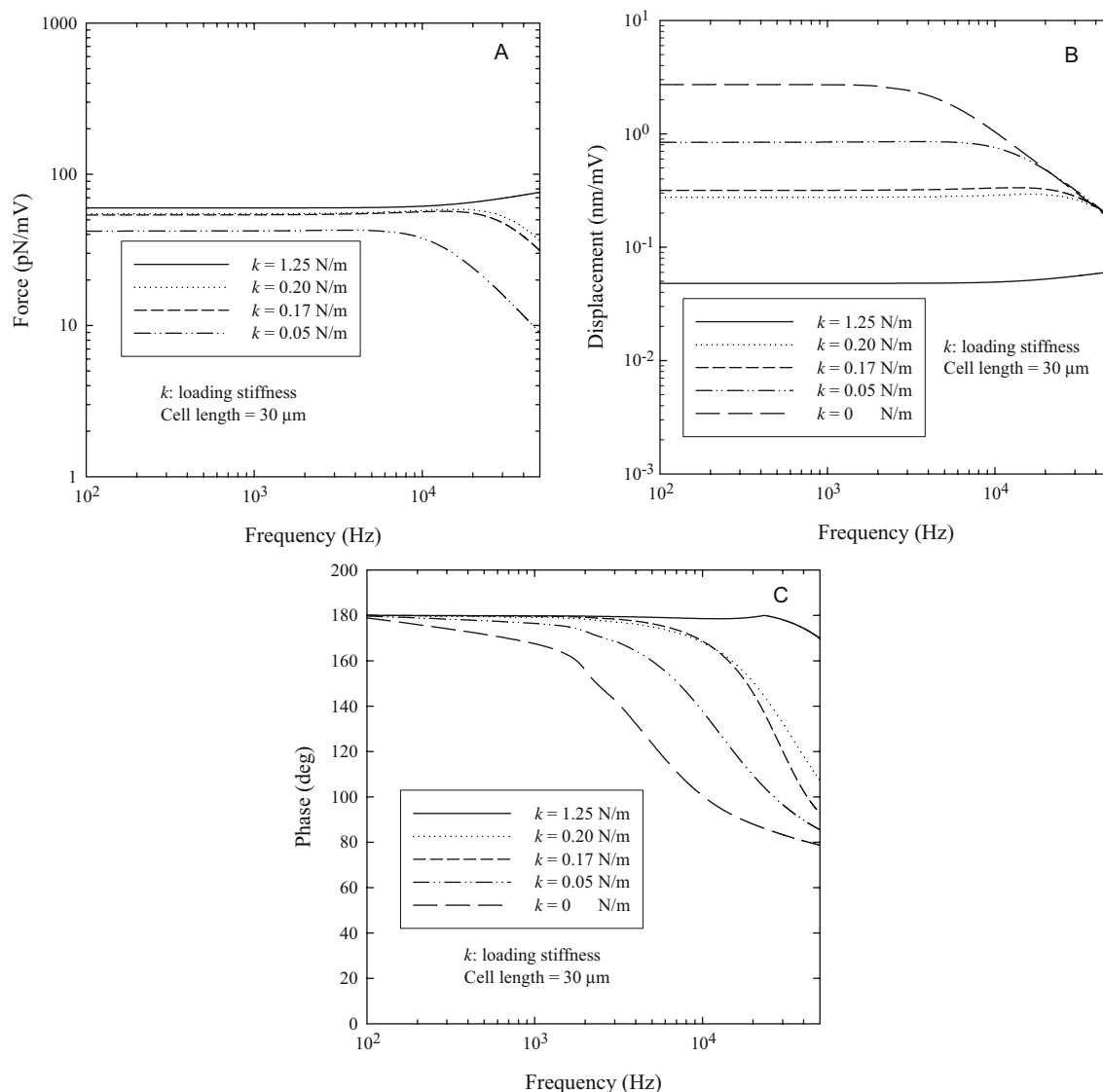Figure 3 shows the force magnitude, displacement, and phase shift for various levels of stiffness of the

FIG. 3. Modeling force generation. (A) Force per unit trans-membrane potential [F_{end} in Eq. (5)], (B) displacement [$|u_{end}|$ in Eq. (5)], (C) phase. Stiffness of the basilar membrane in the basal turn is 1.25 N/m (Gummer et al. 1981), whereas the upper and lower limits of stiffness of the reticular lamina located at the positions of OHCs are 0.20 and 0.05 N/m, respectively (Scherer and Gummer 2004). Stiffness of the tectorial membrane is 0.05 N/m (Kolston, 1999; Zwislocki and Cefaratti 1989). The loading stiffness used in the experiment of Frank et al. (1999) was 0.17 N/m. The near-isometric force can be constant at ~60 pN/mV to 100 kHz, if the basal BM stiffness is chosen. The force here is calculated based on Eq. (5), representing the active force generated by the cell as a result of electrical stimulation.

constraint (spring). To simulate both experimental and physiological conditions, we included a set of curves in which the short-dashed lines correspond to the stiffness of the fiber in the experiment by Frank et al. (1999), and the solid, dotted, and dashed–dotted lines correspond to the stiffness of the cochlear membranes constraining the OHC *in vivo*. The long-dashed line corresponds to the case of a free OHC without the constraint at the cell end. The fiber stiffness in the experiment by Frank et al. (1999) was equal to 0.17 N/m. *In vivo*, OHCs are constrained by the underlying BM and the overlying

TM and RL. Thus, we have estimated the effects of these three components of the cochlea.

The stiffness of the BM in the basal turn of the cochlea was estimated as 1.25 N/m (Gummer et al. 1981), and this case is illustrated by the solid lines in Figure 3. Zwislocki and Cefaratti (1989) and Kolston (1999) estimated the stiffness of the TM as 0.05 N/m. Recently, Scherer and Gummer (2004) probed the organ of Corti along the RL (with the TM removed). The upper and lower limits of the stiffness values obtained were 0.2 and 0.05 N/m, respectively. Assuming that the stiffness of the OHCs underlying

TABLE 2

Model results compared to the experiments of Frank et al. (1999) (low-frequency conditions)

Shift in the membrane potential (mV)	Slope (nm/mV)	e_x/e_θ (N/Vm)	Computed force (pN/mV)	Measured force (pN/mV)
0	4.5	0.0029/0.0018	57.2	13.0
−50	2.2	0.0014/0.00088	28.0	
−100	1.0	0.00064/0.0004	12.7	

The slope is estimated according to Figure 6 of Dallos et al. (1993). It is assumed that e_x/e_θ at two different points changes with corresponding slopes in the same proportion. The measured force is from Frank et al. (1999). Stiffness of the mechanical constraint against the cell end is 0.17 N/m. All forces were determined under low-frequency conditions.

the RL in Scherer and Gummer's (2004) experiment was much smaller than that of the RL, we attribute the stiffness they measured to the RL. Thus, the dotted and dashed–dotted lines in Figure 3 correspond to the upper and lower limits of the stiffness of the RL, respectively. The dashed–dotted lines also represent the case in which the stiffness of the constraint is equal to that of the TM (Zwislocki and Cefaratti 1989; Kolston 1999).

The results presented in Figure 3 demonstrate the importance of the effect of the imposed constraints on the active force produced by the OHC. A more constrained cell had a longer range of constant active force: the ranges of constant active forces reached 30 kHz when the constraint stiffness was 0.17 N/m, as used in the experiment by Frank et al. (1999), and the force reached 100 kHz when the constraint stiffness was equal to that of the basal BM (1.25 N/m).

Our modeling result is in qualitative agreement with the data of Frank et al. (1999), showing a constant force up to several tens of kHz. There is, however, a quantitative difference between the two sets of results that requires explanation: The active force in the experiment by Frank's et al. (1999) was close to 13 pN/mV, which is about four times smaller than our model result (57 pN/mV in Fig. 3A). They pointed out that the set-point in their experiment was not located at the steepest part of the electromechanical transduction function of the OHC. To estimate such a set-point, we selected three points (0, −50, and −100 mV) along the electromechanical transduction curve (Dallos et al. 1993). The slope (sl) at each point can be easily estimated from that curve. We assumed that the coefficient of the electromotile response (e_x or e_θ) changes in proportion to the slope change at two different points (i.e., $e_{x,1}/e_{x,2} = sl_1/sl_2$). As the coefficient of the electromotile response at 0 mV receptor potential is known, the values at the other two points (−50 and −100 mV) can be estimated. Thereafter, the active forces at those two points can be calculated (Table 2). The results showed that if we chose the set-point potential away from the steepest part of the electromechanical transduction function, then our predictions became

much closer to the data of the experiment of Frank et al. (1999).

In terms of estimating the active force production by the OHC *in vivo*, we can reasonably predict that the physiological case lies somewhere between the cases corresponding to stiffness of the BM and that of the RL. In our model, the element attached to the bottom end of the cell represents the BM. In the cochlea, the OHCs interact with the basilar membrane via the supporting DCs. To estimate the effect of DCs on our results, we did an additional analysis in which the attached element reflected the properties of both the basilar membrane and the DC, connected in series. In that analysis, the DC was represented by its mass and stiffness. The relative contribution of these two properties of DC are determined by the ratio $M_D\omega^2/k_D$, where M_D and k_D are the mass and stiffness of the DC, respectively, and ω is the circular frequency of cell vibration. To estimate the mass of the DC, we used the morphological data from Zhao (2005). We approximated the shape of the cell by a prolate spheroid (Laffon and Angelini 1996) and assumed that the cell's density is close to that of the water (10^3 kg/m^3). The stiffness of the DC was estimated as 25 N/m (Tolomeo and Holley 1997). As a result of our analysis, the $M_D\omega^2/k_D$ ratio was found to be below 6% within a 50-kHz frequency range (the hearing range in guinea pigs). Thus, the mass of the DC bears only a small effect when compared to its stiffness. Finally, we compared the effects of the stiffness of the DC and that of the BM. Because the stiffness of DC is about 20 times greater than that of the BM (1.25 N/m), the overall stiffness of the element attached to the bottom end of the outer hair cell is determined by the smaller stiffness of the BM. Thus, in our analysis, the effect of DCs can be neglected.

Our results indicate that the active force produced by the OHC per unit transmembrane potential under physiological conditions is probably constant up to a few tens of kHz. An accurate prediction of the active force production *in vivo* will require a more complete model of the constraints imposed on the OHC, in which all mechanical properties of each of the cell-
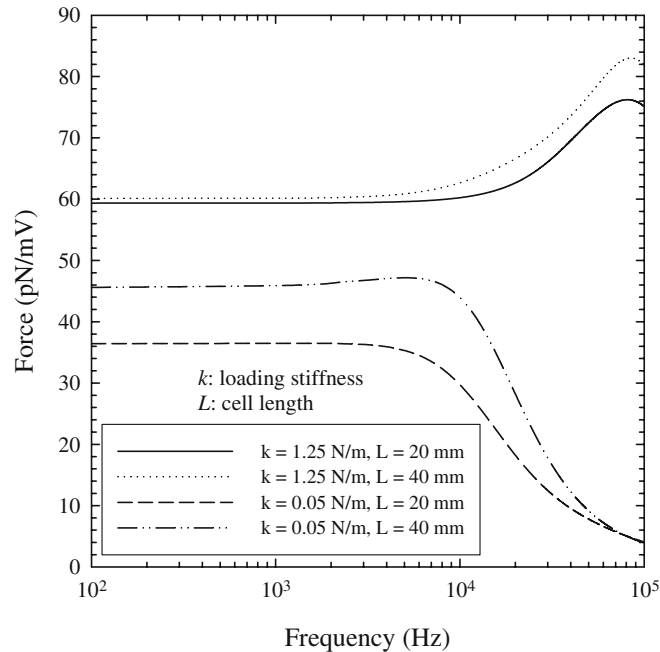
FIG. 4. Effect of cell length on active force generation. Two values, 1.25 and 0.05 N/m, for the stiffness of the constraint are considered, and results are presented for two lengths of cell (20 and 40 μm) for each value of stiffness. The force here is calculated based on Eq. (5), representing the active force generated by the cell as a result of electrical stimulation.

constraining components, BM, TM, and RL, are explicitly considered. Nevertheless, our finding that the constrained OHC generates a greater (up to tens of kHz) range of a constant active force seems consistent with the cochlear frequency map. Indeed, the basal (high-frequency) area of the cochlea associated with the cochlear amplifier has a much greater stiffness of the BM that imposes constraints on OHCs in this area.

Several factors could have contributed to the longer active force plateau under conditions of higher stiffness of the constraint. One is that the higher the stiffness of the constraint, the smaller the movement of the cell (Fig. 3B). Thus, the energy losses associated with the interaction with the two surrounding fluids and with the relative motion of the components of the cell's composite wall become reduced for highly constrained cells. This condition results in a greater roll-off frequency for the force. Another factor is related to the increase in the total stiffness of the system (cell + spring) that also results in an increase in the roll-off frequency.

As we have already noted, we computed the active force per unit cell transmembrane potential. Because physiological receptor potentials are small (a few mV), the total force will be equal to the product of the obtained force per unit transmembrane potential and the receptor potential. Thus, the frequency dependence of the total active force generated by the OHC *in vivo* will be determined by a combination of mechanical factors, which determine cell vibra-

tion, and the electrical (piezoelectric) properties of the cell membrane shaping the receptor potential.

Effect of other parameters

In Figure 4 we analyze the effect of cell length on force production. We have already discussed a weak (or zero) dependence of the isometric force on the cell length (see the section Comparison with previous experimental data) in the case of low frequencies. The isometric conditions correspond to the infinitely large stiffness of the constraint (spring). We have also shown that force has a greater dependence on cell length if the stiffness of the constraint is relatively small (see our discussion of Hallworth's 1995 data above). Our data on the high-frequency case presented in Figure 4 confirmed the tendency found in the low-frequency cases: When the stiffness of the constraint was equal to 0.05 N/m, the force corresponding to a 40-μm cell length was up to ∼30% greater than that corresponding to a 20-μm cell length. The highest difference between the two forces was observed around the corner frequency. The difference in magnitude of the forces corresponding to a stiffness of constraint equal to 1.25 N/m was almost indistinguishable between 20 and 40 μm of cell length.

Figure 5A and B, respectively, show the effect of the cell wall viscosity on the magnitude and phase shift of the active force. For this viscosity, we chose a range between 0 and 4.0×10^{-7} Ns/m (as discussed

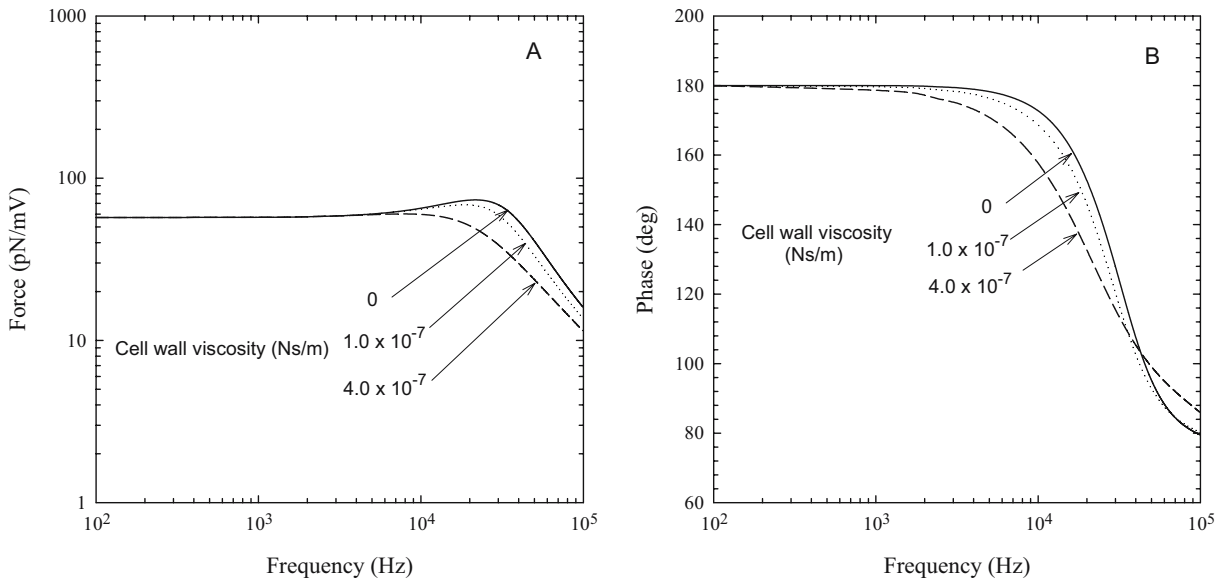**FIG. 5.** Effect of different cell wall viscosities on force generation: (A) amplitude, (B) phase. Cell length is 60 μm and loading stiffness is 0.17 N/m. Internal fluid viscosity is 6.0×10^{-3} Ns/m². The force here is calculated based on Eq. (5), representing the active force generated by the cell as a result of electrical stimulation.

in the section Model parameters). Cell viscosity within the chosen range had a moderate effect on the active force. The roll-off frequencies of both the magnitude and phase shift of the force decreased with the increase in the cell wall viscosity.

Figures 6A and 6B illustrate the effect of the internal fluid viscosity on the magnitude and phase shift of the active force. Three values for internal fluid viscosity (1.0, 6.0, and 10.0×10^{-3} Ns/m²) were investigated. Increase in internal fluid viscosity

resulted in a moderate decrease in the roll-off frequencies of the magnitude and phase shift of the force, which was similar to the effect of cell wall viscosity. The change in internal fluid viscosity noticeably affected the OHC high-frequency force generation but had no effect on force generation in the low-frequency range. In other words, the internal fluid viscosity plays an important role in the high-frequency performance of the OHC, but this effect is negligible in the low-frequency range.
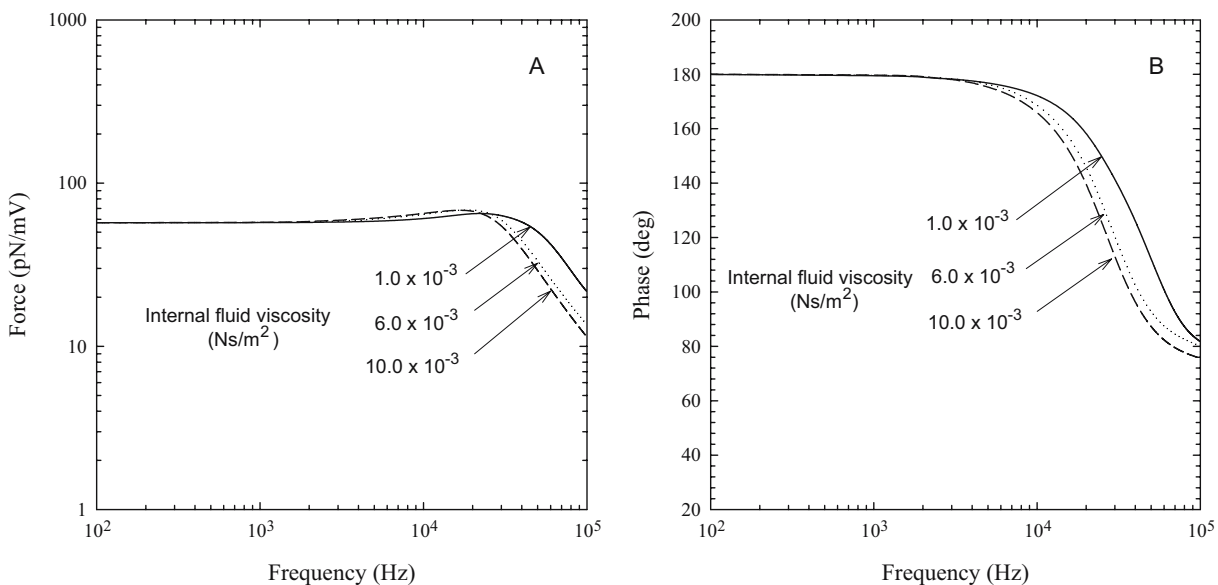

FIG. 6. Effect of different internal fluid viscosities on force generation: (A) amplitude, (B) phase. Cell length is 60 μm and loading stiffness is 0.17 N/m. Cell wall viscosity is 1.0×10^{-7} Ns/m. The force here is calculated based on Eq. (5), representing the active force generated by the cell as a result of electrical stimulation.

CONCLUSIONS

A model of active force generation by OHCs under high-frequency conditions is proposed. This model takes into account the elastic, viscous, and piezoelectric properties of the cell wall, as well as the viscous and inertial properties of the fluids inside and outside the cell. We have also shown that the model is in good agreement with available experimental data for both low and high frequencies. Our findings indicate that the constraints imposed on the cell have a significant effect on the frequency range within which the OHC is capable of producing an almost constant force per unit transmembrane potential. The greater the stiffness of the constraint, the broader the range of the constant active force produced by the cell. We analyzed the OHC response in terms of the stiffness of constraints that are similar to those imposed by the cochlear components (the BM, TM, and RL) that constrain OHCs *in vivo*, and we found that the OHC is capable of generating a constant force per unit transmembrane potential of up to tens of kHz. We also found that cellular characteristics played a role in the range of constant force and force magnitude. The corresponding roll-off frequency decreased when the viscosities of the cell wall and surrounding fluids increased. The magnitude of the active force was increased for longer cells, and the smaller the stiffness of the constraint, the greater was the increase. This model we have developed can be further extended to explicitly include OHC interaction with cochlear components, reflecting their particular properties. Finally, the results we have obtained can expand our understanding of the active processes occurring in the cochlea.

ACKNOWLEDGMENTS

APPENDIX

As shown in Figure 1, the total traction exerted on the cell wall surface is determined by the intracellular and extracellular fluids:

$$\boldsymbol{\sigma}_{\text{cell}} = \boldsymbol{\sigma}_{\text{ext}} - \boldsymbol{\sigma}_{\text{int}}, \tag{A1}$$

where $\boldsymbol{\sigma}_{\text{cell}} = (\sigma_{rx}, \sigma_r)$ is the total traction exerted on the cell wall surface, and σ_{rx} and σ_r are the longitudinal and radial components; $\boldsymbol{\sigma}_{\text{ext}}$ and $\boldsymbol{\sigma}_{\text{int}}$ the are tractions due to the cell's wall interaction with the extracellular and intracellular fluids, respectively.

The equilibrium equations for the cell wall are

$$N_\theta = \sigma_r r_c, \tag{A2}$$

$$N_x = -\int_a^x \sigma_{rx} d\overline{x} + N_{\text{end}} + N_{\text{spring}}, \tag{A3}$$

where r_c is the cell radius, a is the x-axis coordinate of the cell end, and N_{end} and N_{spring} are the resultants generated at the cell end by the closed end and constraint, respectively. The constraint is treated as a spring, and therefore

$$N_{\text{spring}} = -\frac{\boldsymbol{k}_{\text{spring}}}{2\pi r_c} u_{\text{end}}, \tag{A4}$$

where u_{end} is the cell end displacement. The closed end is treated as an oscillatory rigid plate and is subject to fluid resistance, which is transmitted and applied to the cell wall. This force is calculated by

$$N_{\text{end}} = -\frac{\boldsymbol{k}_{\text{end}}}{2\pi r_c} u_{\text{end}}, \tag{A5}$$

where

$$k_{\text{end}} = 16\left[\frac{i\lambda^2}{6} + \left(1.32 e^{i0.27\pi}\lambda\right)\right]\mu r_c(i\omega)e^{i\omega t},$$

and $\lambda^2 = \rho\omega r_c^2/\mu$, where μ is fluid viscosity, ρ is fluid density, ω is circle frequency, and i is $\sqrt{-1}$ (Zhang and Stone 1998). It should be noted that the method we used did not include the complete interaction between the fluid flow, the cell wall, and the cell's closed ends, such as an additional radial stress on the cell wall resulting from the cell ends pushing the intracellular fluid back and forth. However, Tolomeo (1995) did consider the effect of the cell's closed ends and, on the basis of his theoretical approach, found this effect insignificant. In our previous paper (Liao et al. 2005), using a simplified approach, we compared the results for the closed-end and open-end conditions and also found the difference to be insignificant.

The tractions and displacements can be expressed in terms of Fourier series in the cell domain. A symmetric case can be constructed by expanding the excluded part of the cell to the left side of the cell center, just like a mirror reflection. In this case, each radial component can be decomposed into a cosinusoidal series with odd harmonics, while each axial component involves a sinusoidal series with odd harmonics (Weaver 1989; Tolomeo 1995; Tolomeo and Steele 1998):

$$u_x = \sum_{m=\text{odd}}^{m_{\text{max}}} u_{mx} \sin(\beta_m x)e^{i\omega t}, \tag{A6}$$

$$u_r = \sum_{m=\text{odd}}^{m_{\max}} u_{mr} \cos{(\beta_m x)} e^{i\omega t}, \qquad (A7)$$

$$\sigma_{rx} = \sum_{m=\text{odd}}^{m_{\max}} \sigma_{mrx} \sin{(\beta_m x)} e^{i\omega t}, \qquad (A8)$$

$$\sigma_r = \sum_{m=\text{odd}}^{m_{\max}} \sigma_{mr} \cos{(\beta_m x)} e^{i\omega t}, \qquad (A9)$$

$$Ve_x = \sum_{m=\text{odd}}^{m_{\max}} Q_m \cos{(\beta_m x)} e^{i\omega t}, \qquad (A10)$$

$$Ve_\theta = \sum_{m=\text{odd}}^{m_{\max}} P_m \cos{(\beta_m x)} e^{i\omega t}, \qquad (A11)$$

$$N_{\text{end}} = \sum_{m=\text{odd}}^{m_{\max}} S_m \cos{(\beta_m x)} e^{i\omega t}, \qquad (A12)$$

$$N_{\text{spring}} = \sum_{m=\text{odd}}^{m_{\max}} T_m \cos{(\beta_m x)} e^{i\omega t}, \qquad (A13)$$

where $\beta_m = m\pi/L$, L is the whole length of the cell, $Q_m = Ve_x g_m$, $P_m = Ve_\theta g_m$, $S_m = N_{\text{end}} g_m$, $T_m = N_{\text{spring}} g_m$, $g_m = \frac{2(-1)^{\frac{m+1}{2}+1}}{a\beta_m}$ and $m_{\max}$ is the number of harmonics used.

These representations were used to transform the original equations into a form that includes the Fourier coefficients. For example, the application of representations (Eqs. A6–A13) to the constitutive equations (1) results in the following equation for the mth coefficients of the traction and displacement:

$$\begin{bmatrix} \sigma_{mrx} \\ \sigma_{mr} \end{bmatrix} = \begin{bmatrix} (C_{11} + i\omega\eta)\beta_m^2 & (C_{12} - i\omega\eta)\frac{\beta_m}{r_c} \\ (C_{12} - i\omega\eta)\frac{\beta_m}{r_c} & (C_{22} + i\omega\eta)\frac{1}{r_c^2} \end{bmatrix}$$
$$\times \begin{bmatrix} u_{mx} \\ u_{mr} \end{bmatrix} + \begin{bmatrix} Q_m\beta_m \\ \frac{P_m}{r_c} \end{bmatrix} + \begin{bmatrix} -S_m\beta_m \\ 0 \end{bmatrix}$$
$$+ \begin{bmatrix} -T_m\beta_m \\ 0 \end{bmatrix}. \qquad (A14)$$

Denote Eq. (A14) in the form of matrix:

$$\mathbf{F}_{\sigma,m} = \mathbf{k}_{\text{cell},m}\mathbf{F}_{u,m} + \mathbf{F}_{\sigma,m}^{\text{piez}} + \mathbf{F}_{\sigma,m}^{\text{end}} + \mathbf{F}_{\sigma,m}^{\text{spring}}, \qquad (A15)$$

where

$$\mathbf{F}_{\sigma,m} = \begin{bmatrix} \sigma_{mrx} \\ \sigma_{mr} \end{bmatrix}, \ \mathbf{k}_{\text{cell},m}$$
$$= \begin{bmatrix} (C_{11} + i\omega\eta)\beta_m^2 & (C_{12} - i\omega\eta)\frac{\beta_m}{r_c} \\ (C_{12} - i\omega\eta)\frac{\beta_m}{r_c} & (C_{22} + i\omega\eta)\frac{1}{r_c^2} \end{bmatrix}, \mathbf{F}_{u,m} = \begin{bmatrix} u_{mx} \\ u_{mr} \end{bmatrix},$$

$$\mathbf{F}_{\sigma,m}^{\text{piez}} = \begin{bmatrix} Q_m\beta_m \\ \frac{P_m}{r_c} \end{bmatrix}, \ \mathbf{F}_{\sigma,m}^{\text{end}} = \begin{bmatrix} -S_m\beta_m \\ 0 \end{bmatrix}, \ \mathbf{F}_{\sigma,m}^{\text{spring}}$$
$$= \begin{bmatrix} -T_m\beta_m \\ 0 \end{bmatrix}.$$

Eq. (A15) is for only one harmonic. Combining all the harmonics together leads to:

$$\mathbf{F}_\sigma = \mathbf{k}_{\text{cell}}\mathbf{F}_u + \mathbf{F}_\sigma + \mathbf{F}_\sigma^{\text{end}} + \mathbf{F}_\sigma^{\text{spring}}, \qquad (A16)$$

where $\mathbf{F}_\sigma$ and $\mathbf{F}_u$ are vectors of Fourier coefficients of traction on the cell wall surface and cell wall displacement, respectively, i.e., $\mathbf{F}_\sigma = [\sigma_{1rx}\ \sigma_{1r}\ \sigma_{3rx}\ \sigma_{3r}\ \sigma_{5rx}\ \sigma_{5r} \ldots \sigma_{m_{\max}rx}\ \sigma_{m_{\max}r}]^{\text{T}}$, $\mathbf{F}_u = [u_{1x}\ u_{1r}\ u_{3x}\ u_{3r}\ u_{5x}\ u_{5x} \ldots u_{m_{\max}x}\ u_{m_{\max}r}]^{\text{T}}$; T means the transpose of the matrix; $\mathbf{F}_\sigma^{\text{piez}}$, $\mathbf{F}_\sigma^{\text{end}}$, and $\mathbf{F}_\sigma^{\text{spring}}$ are vectors of Fourier coefficients of terms associated with the piezoelectric effect, cell closed end, and spring (constraint).

The force imposed by the closed end on the cell wall (Eq. A5) can take the form (Liao et al. 2005):

$$\mathbf{F}_\sigma^{\text{end}} = \mathbf{k}_{\text{end}}\mathbf{F}_u, \qquad (A17)$$

where $\mathbf{k}_{\text{end}}$ is the generalized stiffness matrix associated with cell's closed end.

Using the same technique (Liao et al. 2005), the force imposed by the constraint on the cell wall (Eq. A4) will take the form:

$$\mathbf{F}_\sigma^{\text{spring}} = \mathbf{k}_{\text{spring}}\mathbf{F}_u, \qquad (A18)$$

where $\mathbf{k}_{\text{spring}}$ is the generalized stiffness matrix associated with the constraint.

Eq. (A1) should still hold for the vector forms of the coefficients of the Fourier series:

$$\mathbf{F}_\sigma = \mathbf{F}_\sigma^{\text{ext}} - \mathbf{F}_\sigma^{\text{int}}, \qquad (A19)$$

where $\mathbf{F}_\sigma$, $\mathbf{F}_\sigma^{\text{ext}}$, and $\mathbf{F}_\sigma^{\text{int}}$ are the vector forms of the coefficients of Fourier expansion of $\boldsymbol{\sigma}_{\text{cell}}$, $\boldsymbol{\sigma}_{\text{ext}}$, and $\boldsymbol{\sigma}_{\text{int}}$, respectively. The right-hand side of the above equation can be related to the cell wall displacement by the following equation (Tolomeo and Steele 1998; Liao et al. 2005):

$$\mathbf{F}_\sigma^{\text{ext}} - \mathbf{F}_\sigma^{\text{int}} = -\mathbf{k}_{\text{fluid}}\mathbf{F}_u. \qquad (A20)$$

Combining Eqs. (A16)–(A20) leads to the following equation:

$$\mathbf{F}_u = -\mathbf{B}^{-1}\mathbf{F}_\sigma^{\text{piez}}, \qquad (A21)$$

where $\mathbf{B} = \mathbf{k}_{\text{cell}} + \mathbf{k}_{\text{fluid}} + \mathbf{k}_{\text{end}} + \mathbf{k}_{\text{spring}}$.

REFERENCES

Brownell WE, Bader CD, Bertrand D, de Ribaupierre Y. Evoked mechanical responses of isolated cochlear outer hair cells. Science 224:194–196, 1985.

DALLOS P, EVANS BN. High frequency motility of outer hair cells and the cochlear amplifier. Science 267:2006–2009, 1995.

DALLOS P, HALLWORTH R, EVANS BN. Theory of electrically driven shape changes of cochlear outer hair cells. J. Neurophysiol. 70:299–323, 1993.

EVANS EA, SKALAK R. Mechanics and Thermodynamics of Biomembranes. CRC Press. Boca Raton, FL, 1980.

FRANK G, HEMMERT W, GUMMER AW. Limiting dynamics of high-frequency electromechanical transduction of outer hair cells. Proc. Natl. Acad. Sci. USA 96:4420–4425, 1999.

FRIDBERGER A, DE MONVEL JB, ZHENG J, HU N, ZOU Y, REN T, NUTTALL A. Organ of Corti potentials and the motion of the basilar membrane. J. Neurosci. 24:10057–10063, 2004.

FUNG YC. Biomechanics: Mechanical Properties of Living Tissues. Springer. Berlin, Heidelberg, New York, 1993.

GALE JE, ASHMORE JF. Charge displacement induced by rapid stretch in the basolateral membrane of guinea-pig outer hair cell. Proc. R. Soc. Lond. B. 255:243–249, 1994.

GOLD T. Hearing. II. The physical basis of the action of the cochlea. Proc. R. Soc. Lond. B. 135:492–498, 1948.

GUMMER AW, JOHNSTONE BM, ARMSTRONG NJ. Direct measurement of basilar membrane stiffness in the guinea pig. J. Acoust. Soc. Am. 70:1298–1309, 1981.

HALLWORTH R. Passive compliance and active force generation in the guinea pig outer hair cell. J. Neurophysiol. 74:2319–2328, 1995.

HALLWORTH R. Modulation of OHC force generation and stiffness by agents known to affect hearing. In: Lewis ER, Long GR, Lyon RF, Narins PM, Steele CR, Hecht-Poinar E (eds) Diversity in Auditory Mechanics. World Scientific. Singapore, pp 524–530, 1997.

HOUSLEY GD, ASHMORE JF. Ionic currents of outer hair cells isolated from the guinea-pig cochlea. J. Physiol. 448:73–98, 1992.

IWASA KH, ADACHI M. Force generation in the outer hair cell of the cochlea. Biophys. J. 73:546–555, 1997.

KOLSTON PJ. Comparing *in vitro, in situ* and *in vivo* experimental data in a three-dimensional model of mammalian cochlear mechanics. Proc. Natl. Acad. Sci. USA 96:3676–3681, 1999.

LAFFON E, ANGELINI E. On the Deiters cell contribution to the micromechanics of the organ of Corti. Hear Res.99:106–109, 1996.

LIAO Z, POPEL AS, BROWNELL WE, SPECTOR AA. Modeling high-frequency electromotility of cochlear outer hair cell in microchamber experiment. J. Acoust. Soc. Am. 117:2147–2157, 2005.

LIBERMAN MC, GAO J, HE DZ, WU X, JIA S, ZUO J. Prestin is required for electromotility of the outer hair cell and for the cochlear amplifier. Nature 419:300–304, 2002.

LUBY-PHELPS K. Cytoarchitecture and physical properties of cytoplasm: volume, viscosity, diffusion, intracellular surface area. Int. Rev. Cytol. 192:189–221, 2000.

MOUNTAIN DC, HUBBARD AE. A piezoelectric model of outer hair cell function. J. Acoust. Soc. Am. 95:350–354, 1994.

OLIVER M, HE DZ, KLOCKER N, LUDWIG J, SCHULTE U, WALDEGGER JP, RUPPENBERG P, DALLOS P, FAKLER B. Intracellular anions as the voltage sensor of Prestin, the outer hair cell motor protein. Science 292:2340–2343, 2001.

OSPECK M, DONG XX, IWASA KH. Limiting frequency of the cochlear amplifier based on electromotility of outer hair cell. Biophys. J. 84:739–749, 2003.

RABBITT RD, AYLIFFE HE, CHRISTENSEN D, PAMARTHY K, DURNEY C, CLIFFORD S, BROWNELL WE. Evidence of piezoelectric resonance in isolated outer hair cells. Biophys. J. 88:2257–2265, 2005.

RATNANATHER JT, SPECTOR AA, POPEL AS, BROWNELL WE. Is the outer hair cell wall viscoelastic? In: Lewis ER, Long GR, Lyon RF, Narins PM, Steele CR, Hecht-Poinar E (eds) Diversity in Auditory Mechanics. World Scientific, Singapore, pp 601–607, 1997.

RYBALCHENKO V, SANTOS-SACCHI J. Cl⁻ flux through a non-selective, stretch-sensitive conductance influences the outer hair cell motor of the guinea-pig. J. Physiol. 547:873–891, 2003.

SANTOS-SACCHI J. On the frequency limit and phase of outer hair cell motility: effects of the membrane filter. J. Neurosci. 12:1906–1916, 1992.

SANTOS-SACCHI J, KAKEHATA S, KIKUCHI T, KATORY Y, TAKASAKA T. Density of motility-related charge in the outer hair cell of the guinea pig is inversely related to best frequency. Neurosci. Lett. 256:155–158, 1998.

SCHERER MM, GUMMER AW. Impedance analysis of the organ of Corti with magnetically actuated probes. Biophys. J. 87:1378–1391, 2004.

SPECTOR AA, JEAN RP. Elastic moduli of the piezoelectric cochlear outer hair cell membrane. Exp. Mech. 43:355–360, 2003.

SPECTOR AA, BROWNELL WE, POPEL AS. Estimation of elastic moduli and bending stiffness of the anisotropic outer hair cell wall. J. Acoust. Soc. Am. 103:1007–1011, 1998.

SPECTOR AA, BROWNELL WE, POPEL AS. Nonlinear active force generation by cochlear outer hair cell. J. Acoust. Soc. Am. 105:2414–2420, 1999.

SPECTOR AA, BROWNELL WE, POPEL AS. Effect of the membrane piezoelectric properties on the outer hair cell receptor potential under high-frequency conditions, In: Abstracts of the 29th Meeting of ARO, St. Petersburg Beach, FL, pp 255, 2002.

SPECTOR AA, BROWNELL WE, POPEL AS. Effect of outer hair cell piezoelectricity on high-frequency receptor potentials. J. Acoust. Soc. Am. 113:453–461, 2003.

STEELE CR, BAKER G, TOLOMEO JA, ZETES D. Electromechanical models of outer hair cell. In: Duifhuis H, Horst JW, van Dijk P, van Netten SM (eds) Biophysics of Hair Cell Sensory Systems. World Scientific, Singapore, pp 207–214, 1993.

TOLOMEO JA. Models of the structure and motility of the auditory outer hair cell. Ph.D. thesis, Stanford University. 1995.

TOLOMEO JA, HOLLEY MC. The function of the cytoskeleton in determining the mechanical properties of epithelial cells within the Organ of Corti. In: Lewis ER, Long GR, Lyon RF, Narins PM, Steele CR, Hecht-Poinar E (eds) Diversity in Auditory Mechanics. World Scientific, Singapore, pp 556–562, 1997.

TOLOMEO JA, STEELE CD. A dynamic model of outer hair cell motility including intracellular and extracellular viscosity. J. Acoust. Soc. Am. 103:524–534, 1998.

WEAVER HJ. Theory of Discrete and Continuous Fourier Analysis. Wiley, New York, 1989.

WEITZEL EK, TASKER R, BROWNELL WE. Outer hair cell piezoelectricity: frequency response enhancement and resonance behavior. J. Acoust. Soc. Am. 114:1462–1466, 2003.

ZHANG W, STONE HA. Oscillatory motions of circular disks and nearly spherical particles in viscous flows. J. Fluid Mech. 367:329–358, 1998.

ZHAO HB. Connexin26 is responsible for anionic molecule permeability in the cochlea for intercellular signalling and metabolic communications. Eur J Neurosci. 21:1859–1868, 2005.

ZHENG J, SHEN W, HE DZ, LONG KB, MADISON LD, DALLOS P. Prestin is the motor protein of cochlear outer hair cell. Nature (London). 405:149–155, 2000.

ZWISLOCKI JJ, CEFARATTI JK. Tectorial membrane II: stiffness measurements *in vivo*. Hearing Res. 42:211–227, 1989.